J. Fluid Mech. (1974), *vol.* 66, *part* 1, *pp.* 145–157
Printed in Great Britain

Boundary-layer-induced potential flow on an elliptic cylinder

By STANLEY G. RUBIN AND FRANK J. MUMMOLO
Preston R. Bassett Research Laboratory, Polytechnic Institute of New York, Farmingdale

(Received 27 October 1972 and in revised form 25 February 1974)

The application of slender-body theory to the evaluation of the three-dimensional surface velocities induced by a boundary layer on an elliptic cylinder is considered. The method is applicable when the Reynolds number is sufficiently large so that the thin-boundary-layer approximation is valid. The resulting potential problem is reduced to a two-dimensional consideration of the flow over an expanding cylinder with porous boundary conditions. The limiting solutions for a flat plate of finite span and a nearly circular cross-section are obtained in a simple analytic form. In the former case, within the limitations of slender-body theory, the results are in exact agreement with the complete three-dimensional solution for this geometry.

1. Introduction

Three-dimensional potential flow fields induced by boundary layers, in particular on surfaces with locally large or even infinite transverse curvature,† are extremely difficult to determine by analytic or even numerical methods. Only a limited group of analyses, for very specific geometries, is at present available. These include the quarter-plate investigations of Stewartson & Howarth (1970) and Stewartson (1961) and the cruciform studies of Rubin (1966), Pal & Rubin (1971) and Rubin & Grossman (1971).

One of the difficulties associated with the determination of boundary-layer interactions of this type is the complexity of the three-dimensional potential problem that arises when the displacement-induced flow field is to be evaluated. From this potential-flow solution, boundary-layer-induced velocities are determined. With a systematic application of singular perturbation methods, the induced velocity distributions along the surface become the necessary asymptotic matching conditions for the cross-flow boundary-layer analysis, as well as for higher-order boundary-layer considerations. The cross-flow direction is defined here to be along the surface and normal to the direction of the undisturbed stream, i.e. in the direction of ω in figure 1.

Since the cross-flow and second-order boundary-layer analyses require, as asymptotic boundary conditions, only the potential velocities evaluated along

† That is, when the local cross-sectional curvature multiplied by the local boundary-layer thickness is $O(1)$ or larger.

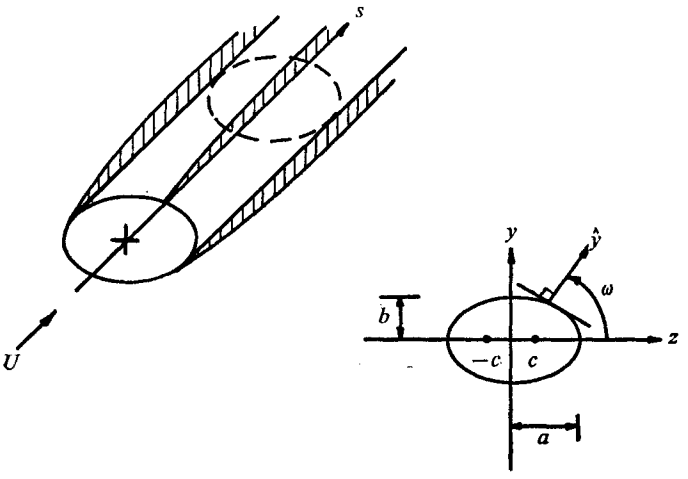

FIGURE 1. Flow geometry.

the surface, the slender-body theory of Munk, Jones & Ward, for many years a powerful approximation in inviscid aerodynamic theory, is adapted here to treat high Reynolds number incompressible flow over an elliptic cylinder.

If the Reynolds number $R_a = Ua/\nu$ based on free-stream values and a typical body dimension a, see figure 1, is assumed to be large, a thin boundary layer develops over the cylinder. Furthermore, if the transverse curvature of the cylinder is nowhere large, to lowest order in a curvature parameter Δ^*/a a Blasius boundary layer with thickness $\Delta^* \sim s^{\frac{1}{2}}$ forms along the generators of the cylinder (Cooke 1957). This solution is independent of the azimuthal angle ω and exhibits zero cross-flow velocity. Δ^* is the displacement thickness defined as

$$\Delta^* \equiv \int_0^\infty \left(1 - \frac{u}{U}\right) d\hat{y}, \tag{1}$$

where u is the local velocity in the s co-ordinate direction, measured along the undisturbed stream, and y is measured locally normal to the surface; see figure 1.

Boundary regions with locally large or infinite transverse curvature such as occur at the edges of a highly eccentric elliptic cross-section or in the flow near a blunted nose cap attached to the cylinder must be treated separately by local singular perturbation analyses; see Rubin (1966) and Van Dyke (1964). For the downstream flow considered here, the effect of the nose is assumed to be small; see Seban & Bond (1951).

The boundary-layer-induced potential flow is determined from the solution of the mass-continuity and irrotationality equations of the inviscid flow. Therefore the perturbation velocity potential ϕ satisfies

$$\phi_{ss} + \phi_{yy} + \phi_{zz} = 0, \tag{2}$$

where y and z denote the cross-plane directions (see figure 1).

The surface boundary layer perturbs the outer inviscid flow in much the same way as does a streamwise variation in body cross-sectional area. An 'effective

slender body' of slowly varying cross-sectional area is formed by the cylinder plus the boundary-layer displacement thickness Δ^*. From slender-body theory, see Ward (1955, p. 195), a first approximation to (2) valid in the vicinity of the body surface is known to be

$$\hat{\phi}_{yy} + \hat{\phi}_{zz} = 0. \tag{3}$$

This reduction is possible locally if discontinuities in streamwise or azimuthal curvature do not appear, and if the body is slender in the sense that the typical cross-sectional dimension is small compared with the longitudinal dimension l or distance s.

If a thin Blasius boundary layer forms on the cylinder, then $\Delta^*/a \ll 1$, where $\Delta^*/s = O(R_s^{-\frac{1}{2}})$ and $R_s = R_a s/a$. Therefore, the boundary-layer plus slender-body conditions lead to the following range of validity for the present theory:

$$1 \ll s/a \ll R_a. \tag{4}$$

The general solution of (3) is of the form

$$\hat{\phi}(s, y, z) = \hat{\phi}_1(y, z;\, s) + b_0(s), \tag{5a}$$

where, for the incompressible flow considered here,

$$b_0(s) = \frac{S'(s)}{4\pi} \ln\left[(4s)\,(l-s)\right]^{-1} - \frac{1}{4\pi}\int_0^l \frac{S'(x) - S'(s)}{|s-x|}\,dx. \tag{5b}$$

$S(s)$ denotes the local cross-sectional area of body of length l, and in the present context can be interpreted as a modified cross-section, taken to include the displacement boundary layer. Therefore, the original three-dimensional potential problem (2) is replaced by a much simpler two-dimensional problem (3) for the boundary-layer-induced flow.

The error in the approximate solution (3) can be assessed by evaluating the Poisson equation for the next-order perturbation potential $\phi^{(1)}$ due to the neglected $\phi^{(0)}_{ss}$ term. This procedure is discussed briefly in Ashley & Landahl (1965, p. 99) and Ward (1955, p. 196). An analysis for an axisymmetric circular cylinder plus displacement layer leads to a relative error $\phi^{(1)}_s/\phi^{(0)}_s = O((a/s)^2)$. This is small in the region of validity of the present analysis as given by (4).

The surface boundary conditions for (3) are obtained by asymptotic matching with the inner boundary layer. For large R_s, in the usual boundary-layer sense, this condition is applied at the surface of the cylinder. At large distances from the cylinder free-stream conditions are approached and the perturbation velocities vanish.

The details of the analysis are presented in the next section for incompressible viscous flow over a cylinder with constant elliptic-cross-section; see also Rubin & Mummolo (1973). The complete solution is described in terms of the eccentricity e and the axisymmetric ($e = 0$) and flat-plate ($e = 1$) limits are obtained. A particularly simple form of the solution results for cross-sections that are nearly circular ($e \ll 1$). The flat-plate limit is compared with the three-dimensional solution obtained from an extension of the quarter-plate analysis of Stewartson & Howarth (1960).

2. Solution for an elliptic cylinder

Consider incompressible flow over a cylinder of constant elliptic cross-section. The generators of the cylinder are taken parallel to the free stream with $l > s > 0$ (figure 1). The Reynolds number based on the semi-major axis is sufficiently large that boundary-layer theory applies in the usual manner. It is assumed here that the transverse curvature of the cross-section is small with respect to the boundary-layer thickness. At the ends of a highly eccentric elliptic cross-section or, in a limiting case, at the edges of a plate of zero thickness this condition is violated locally and singular boundary regions appear. However, to lowest order in $R_s^{-\frac{1}{2}} \ll 1$, the viscous boundary regions do not affect the flow behaviour in the adjoining quasi-two-dimensional boundary layers or the outer inviscid potential flow (see Rubin 1966).

The lowest-order boundary-layer solution due to Cooke (1957), valid downstream of a leading edge or nose region and away from boundary regions, is identical with the constant-pressure flat-plate boundary-layer results of Blasius; see Van Dyke (1964, p. 129). Transverse curvature enters only in higher-order approximations. It is sufficient to note here that the displacement velocity v normal to the surface induced by viscosity has the following asymptotic behaviour for large values of the boundary-layer variable $\eta = \hat{y}(U/2\nu s)^{\frac{1}{2}}$:

$$\lim_{\eta\to\infty}\{v(s,\eta)/U\} \sim 0{\cdot}860/R_s^{\frac{1}{2}}. \tag{6a}$$

The displacement thickness Δ^* as defined in (1) is given by

$$\Delta^* = 1{\cdot}72s/R_s^{\frac{1}{2}}. \tag{6b}$$

For large Reynolds numbers $R_s \gg 1$ the inviscid outer flow is only slightly perturbed by the formation of the thin boundary layer on the surface and therefore the solution for the incompressible displacement-induced potential flow can be determined from (3).

A far-field velocity decay condition

$$\nabla_{2D}\hat{\phi} \to 0 \tag{7a}$$

applies at large distances from the body and a smooth match with the inner boundary layer must be prescribed. ∇_{2D} is the two-dimensional gradient operator in the y, z plane. The surface matching condition is specified by

$$\lim_{\hat{y}\to 0}\{\mathbf{n}.\nabla_{2D}\hat{\phi}(s,\hat{y},\omega)\} = \lim_{\eta\to\infty}\{v/U\} \sim 0{\cdot}860/R_s^{\frac{1}{2}}, \tag{7b}$$

where $\mathbf{n}$ is the unit vector normal to the surface in the y, z plane.

In general, the solution of (3) satisfying (7) can be investigated with conformal mapping techniques. Since only an elliptic cross-section is considered here, it is convenient to transform directly to an elliptic co-ordinate frame. The general solution for the 'two-dimensional' potential $\hat{\phi}$ in this co-ordinate frame is then

$$\hat{\phi} = a_0(s)\,\xi + c_0(s) + \sum_{n=1}^{\infty} a_n(s)\,e^{-n\xi}\cos n\theta, \tag{8}$$

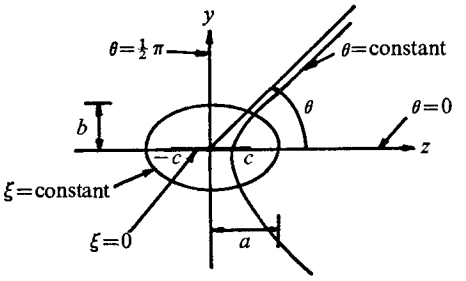

FIGURE 2. Elliptic co-ordinates. $0 \leqslant \xi < \infty$, $0 \leqslant \theta < 2\pi$.

where (ξ, θ) are elliptic co-ordinates (see figure 2) defined by

$$z = c\cosh\xi\cos\theta, \quad y = c\sinh\xi\sin\theta, \tag{9a,b}$$

$$r^2 = y^2+z^2, \quad \omega = \tan^{-1}(y/z), \tag{9c}$$

$$\xi = \ln\frac{r}{c}+\tfrac{1}{2}\ln\left\{1+\left[\left(1-\frac{c^2}{r^2}\right)^2+4\left(\frac{c}{r}\right)^2\sin^2\omega\right]^{\frac{1}{2}} + \left[2\left(1-\left(\frac{c^2}{r^2}\right)\cos 2\omega+\left\{\left(1-\frac{c^2}{r^2}\right)^2+4\left(\frac{c^2}{r^2}\right)\sin^2\omega\right\}^{\frac{1}{2}}\right)\right]^{\frac{1}{2}}\right\}, \tag{9d}$$

with $c^2 = a^2-b^2$ and $e = c/a = (\cosh\xi)^{-1}$, where a and b are the lengths of the semi-major and semi-minor axes, respectively, and e is the eccentricity of the elliptic section.

The boundary condition (7*b*) becomes

$$\lim_{\xi\to\xi_0}[c\,(\cosh^2\xi-\cos^2\theta)^{\frac{1}{2}}]^{-1}\,\partial\phi(\xi,\theta;s)/\partial\xi = (0{\cdot}860/R_a^{\frac{1}{2}})\,(a/s)^{\frac{1}{2}} = d\Delta^*/ds, \tag{10}$$

where the surface is denoted by the ellipse $\xi = \xi_0$.

The coefficients a_n are defined by

$$a_0 = \frac{1}{2\pi}\int_0^{2\pi}\frac{\partial\phi}{\partial\xi}(\xi_0,\theta;s)\,d\theta, \tag{11a}$$

$$a_n = \frac{-2e^{-n\xi_0}}{n\pi}\int_0^{\pi}\frac{\partial\phi}{\partial\xi}(\xi_0,\theta;s)\cos n\theta\,d\theta, \tag{11b}$$

where $\partial\phi(\xi_0,\theta;s)/\partial\xi$ is determined from (10). The coefficient $2\pi a_0$ can be shown to represent the streamwise (s) derivative of the 'effective' cross-sectional surface area of the cylinder formed by the ellipse plus the displacement layer of thickness Δ^* and denoted here as $S'(s)$.† This result is exact when the boundary condition (7*b*) is satisfied at the displacement surface. In general, when the boundary condition is transferred to the surface, as given by (10), a_0 differs from $S'(s)$ by a term of order $(\Delta^*/a)^2$. This difference is negligible in the present analysis but would reappear if higher-order solutions for the outer inviscid flow were considered. Therefore, the surface-area terms $S'(s)$ in (5) are represented by

$$S'(s) = 2\pi a_0 = \left\{\lim_{\xi\to\xi_0}\int_0^{2\pi} c\,(\cosh^2\xi-\cos^2\theta)^{\frac{1}{2}}\,d\theta\right\}\frac{d\Delta^*}{ds} \tag{12}$$

or

$$S'(s) = 4aE(\tfrac{1}{2}\pi, e)\,d\Delta^*/ds, \tag{12a}$$

† This result can easily be proved by a mass conservation argument.

where E is a complete elliptic integral of the second kind, defined in Gradshteyn & Ryzhik (1965, p. 909).

Two limiting cases are the following.

(i) For a circle of radius a, $c \to 0$ and $c \cosh \xi_0 \to a$, so that

$$S'(s) = 2\pi a \, d\Delta^*/ds. \tag{12b}$$

(ii) For a flat plate of span $2a$, $b \to 0$, $c \to a$, $\xi_0 \to 0$ and (12a) gives

$$S'(s) = 4a \, d\Delta^*/ds. \tag{12c}$$

The coefficient $c_0(s)$ in (8) is defined so that the expressions (5) obtained by Ward (1955, p. 199) are applicable in that form; see Kahane & Solarski (1953).

$$c_0(s) = a_0(s) \ln \tfrac{1}{2}c.$$

Therefore, using (5) and (10)–(12) and noting that odd coefficients a_{2n+1} vanish, the solution for $\hat{\phi}$ becomes

$$\hat{\phi}(s, \xi, \theta) = \frac{S'(s)}{2\pi}\left(\xi + \ln\frac{c}{2}\right) + b_0(s) - \frac{+1{\cdot}72c}{\pi R_s^{\frac{1}{2}}} \sum_{n=1}^{\infty} \frac{\exp[-2n(\xi - \xi_0)]}{n} \times \left\{\int_0^{\frac{1}{2}\pi} (\cosh^2 \xi_0 - \cos^2 \beta)^{\frac{1}{2}} \cos 2n\beta \, d\beta\right\} \cos 2n\theta. \tag{13}$$

The induced velocities at the surface $\xi = \xi_0$ of the ellipse are

$$\frac{u}{U} = \hat{\phi}_s = \frac{-0{\cdot}860}{\pi R_a^{\frac{1}{2}}}\left(\frac{a}{s}\right)^{\frac{3}{2}}\left[\left\{\ln\left(\frac{a}{16s}\right)[1 + (1-e)^{\frac{1}{2}}] + 2\right\} E\left(\frac{\pi}{2}, e\right) - \sum_{n=1}^{\infty} \frac{\cos 2n\theta}{n}\left\{\int_0^{\frac{1}{2}\pi} (1 - e^2 \cos^2 \beta)^{\frac{1}{2}} \cos 2n\beta \, d\beta\right\}\right], \tag{14a}$$

$$\frac{w}{U} = a^{-1}(1 - e^2 \cos^2 \theta)^{-\frac{1}{2}} \hat{\phi}_\theta = \frac{3{\cdot}44}{\pi R_a^{\frac{1}{2}}}\left(\frac{a}{s}\right)^{\frac{1}{2}} \sum_{n=1}^{\infty} \frac{\sin 2n\theta}{(1 - e^2 \cos^2 \theta)^{\frac{1}{2}}} \int_0^{\frac{1}{2}\pi} (1 - e^2 \cos^2 \beta)^{\frac{1}{2}} \cos 2n\beta \, d\beta. \tag{14b}$$

Previous boundary-layer analyses of transverse curvature effects on cylinders of circular and more general cross-section have erroneously neglected these displacement-induced boundary conditions, e.g. Cooke (1957) and Seban & Bond (1951). A discussion of the errors arising from the neglect of these displacement effects for the case of a circular cylinder was given by Van Dyke (1970). The complete boundary-layer analysis is currently under way.

For the remainder of the present paper, the solutions (14) for the induced velocities will be discussed for varying eccentricities. The limiting circular and flat-plate results will be obtained for comparison with known exact solutions. This will establish the validity of the application of slender-body theory to the boundary-layer-induced potential problem considered herein and serve as a model for examinations of more complex cross-sections for which exact three-dimensional solutions are not at present available.

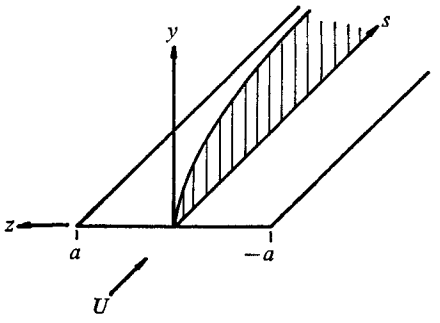

FIGURE 3. Flat-plate geometry.

2.1. *Flat plate*

The flat plate is the simplest geometry for which displacement-induced cross-flows appear. With the formulation presented herein, the surface velocities can be evaluated from the general solution (14) for the elliptic cylinder by the limiting process $\xi_0 \to 0$, $c \to a$. The solution for a flat plate can also be found directly using the quasi-two-dimensional slender-body theory discussed here or a complete three-dimensional formulation. This latter approach has been considered by Stewartson & Howarth (1960) for a quarter-infinite flat plate and is readily extended to the finite-span case.

Consider a plate of span $2a$ as shown in figure 3. Away from the side edge boundary regions, a Blasius boundary layer forms on the plate. The induced velocities at the surface can be obtained by a simple extension of the three-dimensional method of Stewartson & Howarth (1960).

On the plate $y = 0$, *with* $a/s \ll 1$, the cross-flow velocity takes the form

$$\left.\frac{w}{U}\right|_{y=0} \sim \frac{-0{\cdot}860}{\pi R_s^{\frac{1}{2}}} \ln\left[\frac{a-z}{a+z}\right]. \tag{15a}$$

Along the plate centre-line $y = z = 0$ and *with* $a/s \ll 1$, the streamwise perturbation becomes

$$\left.\frac{u}{U}\right|_{y=z=0} \sim \frac{-0{\cdot}860}{\pi R_s^{\frac{1}{2}}} \left[\frac{a}{s}\left(\ln\frac{a}{8s}+1\right)\right], \tag{15b}$$

while at the plate edge we obtain

$$\left.\frac{u}{U}\right|_{y=0,\,z=a} \sim \frac{-0{\cdot}860}{\pi R_a^{\frac{1}{2}}} \left(\frac{a}{s}\right)^{\frac{3}{2}} \left[\ln\frac{a}{4s}+1\right]. \tag{15c}$$

The flat-plate limit is obtained from the general solution (14) for the elliptic cylinder by setting $\xi_0 \equiv 0$ and noting from (12*c*) that

$$a_0(s) = \frac{2a}{\pi}\frac{d\Delta^*}{ds} = \frac{S'(s)}{2\pi}.$$

The streamwise perturbation velocity (14a) on the plate centre-line $\theta = \frac{1}{2}\pi$ becomes

$$\left.\frac{u}{U}\right|_{y=z=0} = \frac{S''}{2\pi}\left[\ln\frac{a}{2} + \sum_{n=1}^{\infty}\frac{(-1)^n}{n(4n^2-1)}\right] + b_0'(s)\dagger$$

$$= \frac{-0{\cdot}860}{\pi R_s^{\frac{1}{2}}}\left(\frac{a}{s}\right)\left[\ln\frac{a}{8s}+1\right]. \tag{16}$$

At the edge, (15c) is recovered. See Gradshteyn & Ryzhik (1965, p. 46).

The cross-flow on the plate is given by

$$\left.\frac{w}{U}\right|_{y=0} = \frac{-S'(s)}{\pi a|\sin\theta|}\sum_{n=1}^{\infty}\frac{\sin 2n\theta}{4n^2-1}.$$

It is easily shown that

$$\frac{4}{|\sin\theta|}\sum_{n=1}^{\infty}\frac{\sin 2n\theta}{4n^2-1} = \ln\left(\frac{a-z}{a+z}\right),$$

where from (9b) $z = a\cos\theta$. Therefore

$$\left.\frac{w}{U}\right|_{y=0} = \frac{-0{\cdot}860}{\pi R_s^{\frac{1}{2}}}\ln\left(\frac{a-z}{a+z}\right). \tag{17}$$

The results (16) and (17) are in exact agreement with the leading terms in the three-dimensional solutions (15).

The slender-body solution for the induced velocities on a flat plate has also been determined by direct application of a two-dimensional Green's function. Equations (15) are recovered (see Rubin & Mummolo 1973).

2.2. *Quasi-axisymmetric flow*

For geometries where the cross-sections are nearly circular ($e \ll 1$), the leading terms in an expansion of (14) for small e take a particularly simple form. We find that

$$\left.\frac{u}{U}\right|_{\xi=\xi_0} = \frac{-0{\cdot}430}{R_a^{\frac{1}{2}}}\left(\frac{a}{s}\right)^{\frac{3}{2}}\left[\left(1-\frac{e^2}{4}\right)\left\{\left(1-\frac{e^2}{4}\right)\ln\frac{a}{8s}+2\right\}+\frac{e^2}{8}\cos 2\theta\right]+O(e^4) \tag{18a}$$

and

$$\left.\frac{w}{U}\right|_{\xi=\xi_0} = \frac{-0{\cdot}215}{R_a^{\frac{1}{2}}}\left(\frac{a}{s}\right)^{\frac{1}{2}}e^2\sin 2\theta + O(e^4), \tag{18b}$$

where from (12)

$$S'(s) = (1{\cdot}72\pi a/R_a^{\frac{1}{2}})(1-\tfrac{1}{4}e^2)+O(e^4).$$

The relation

$$\int_0^{\frac{1}{2}\pi}\cos^{2m}x\cos 2nx\,dx = \begin{cases} 0 & \text{for } m<n \\ \dfrac{\pi}{2^{2m+1}}\dbinom{2m}{m-n} & \text{for } m\geqslant n \end{cases}$$

has been used to obtain (18b) and is useful if additional terms in the expansion are desired. The series in (14) reduce to n terms for the e^{2n} coefficient. The expressions (18) are valid for $e \ll 1$ and will be compared with the general solutions, for arbitrary e, to be discussed in the following section. The axisymmetric solutions

† Here $b_0'(s)$ denotes the derivative of (5b) in the limit $l \to \infty$.

($e = 0$) have previously been obtained by Van Dyke (1970), who also discussed the second-order boundary layer and corrected an earlier paper by Seban & Bond (1951).

Finally, the special limiting case $a \to \Delta^*$, $e \to 0$ of a needle leads to the flow over a slender paraboloid of revolution. While the Blasius boundary layer is incorrect in this limit (see Glauert & Lighthill 1955), the exact solution for a paraboloid is known and provides an additional check on the theory (Van Dyke 1964, p. 75). With the cylindrical radius defined by

$$R_0(s) = (2\epsilon^2 s)^{\frac{1}{2}}$$

Van Dyke has shown that $\phi = \frac{1}{2}\epsilon^2 \ln(r^2/2\epsilon^2 s)$

and
$$\frac{u}{U} = -\frac{\epsilon^2}{2s} = -\frac{R_0}{2s}\frac{dR_0}{ds}. \tag{19}$$

From (5), (14a) and (12b) with $a = \Delta^*$, we obtain for $l \to \infty$

$$\frac{u}{U} = b_0'(s) = -\frac{\Delta^*}{2s}\frac{d\Delta^*}{ds}. \tag{20}$$

With the cylindrical radius $R_0(s)$ set equal to the effective body radius or displacement thickness Δ^* we see that (19) and (20) are identical.

2.3. *Elliptic cylinder*

The flow properties at the surface of a cylinder of elliptic cross-section with arbitrary eccentricity e have been determined by numerical evaluation of an appropriate number of terms in the series solutions (14). The integrals in (14) can be expressed by means of recursion relations in terms of elliptic integrals of the first and second kind; see Gradshteyn & Ryzhik (1965, p. 159). It was more convenient to evaluate the integrals directly by numerical integration. A three-point Simpson's rule having a nominal error of order h^4 was used; h represents the grid spacing. As n increases, the integrand exhibits rapid oscillations and an increased number of mesh points is required. In order to maintain a fixed error, twelve intervals were always located between the zeros of $\cos 2n\theta$, so that $24N + 1$ points result for $n = N$.

The number N of terms required to achieve a specified degree of accuracy increases sharply as $e \to 1$. The summation was terminated when percentage differences in the sums of S and $S + 5$ terms were less than 10^{-10}. The singular behaviour in the flat-plate limit and in particular near the side edge is not unexpected. For $e = 1$ a logarithmic singularity in the cross-flow velocity (14b) appears at the edge, while for $e < 1$, $w \to 0$. Also, the asymptotic form of the integrals in (14) shows that $e = 1$ is a singular limit, since

$$\lim_{n\to\infty} \int_0^{\frac{1}{2}\pi} (1 - e^2\cos^2\theta)^{\frac{1}{2}} \cos 2n\theta \, d\theta \sim \begin{cases} o(A(e))\, n^{-M} & \text{for any finite } M > 0 \text{ with } e < 1, \\ -(4n^2 - 1)^{-1} & \text{for } e = 1. \end{cases}$$

The asymptotic form for $e = 1$ is also obvious from the exact solution (15a).

The numerical solutions for the cross-flow velocity are depicted in figure 4 and confirm the asymptotic predictions. Note the large increase in the maximum

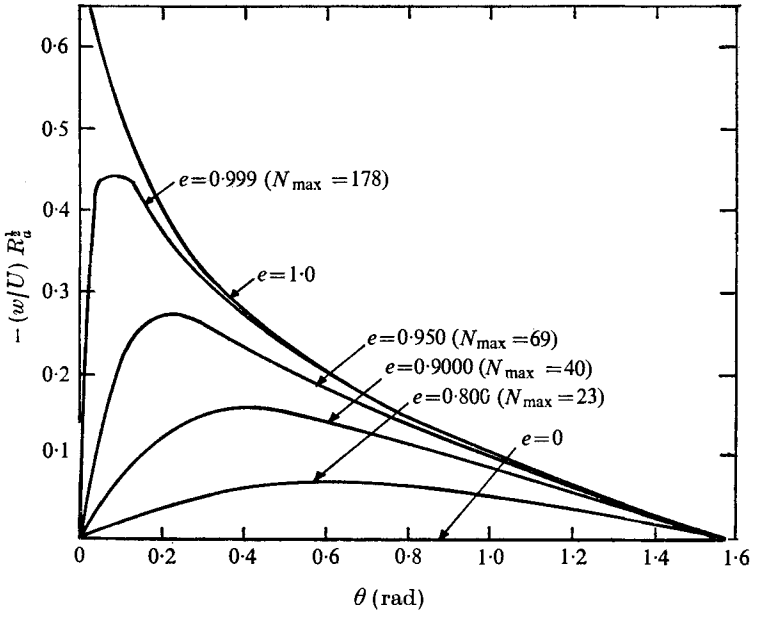

FIGURE 4. Cross-flow. $a/s = 0{\cdot}1$.

number N_{max} of terms required for the series solution as $e \to 1$. For $e = 0{\cdot}999$, the solution closely follows the flat-plate logarithmic behaviour before falling rapidly near the edge. The solution exhibits boundary-layer behaviour near the edge, the peak cross-flow velocity approaching the edge as $e \to 1$. The maximum number of terms required for the series summation generally occurs at a location corresponding to the peak w value. A boundary region forms near the edge and the three-dimensional viscous flow must be re-evaluated.

Similar behaviour for the streamwise velocity perturbation is shown in figure 5. While the streamwise velocity distribution is continuous as $e \to 1$, the velocity gradient also exhibits a logarithmic singularity. Also depicted on figures 4 and 5 are solutions for several values of e between zero and one. The simple quasi-axisymmetric expansions for $e \ll 1$ are given by (18a) and (18b) and are shown in figures 6 and 7. The one-term expansions agree quite well with the numerical solutions for $e \leqslant 0{\cdot}25$.

3. Summary

In order to analyse the perturbation velocities, and in particular the cross-flows induced by thin boundary layers on three-dimensional bodies, a difficult potential problem must be solved. To date, there are only a very small number of such exact solutions available. When considering the flow over an elliptic cylinder, it has been shown herein that slender-body theory, for many years a powerful tool of classical aerodynamics, can be adapted for the determination of the boundary-layer-induced potential flow. In essence, the potential problem is

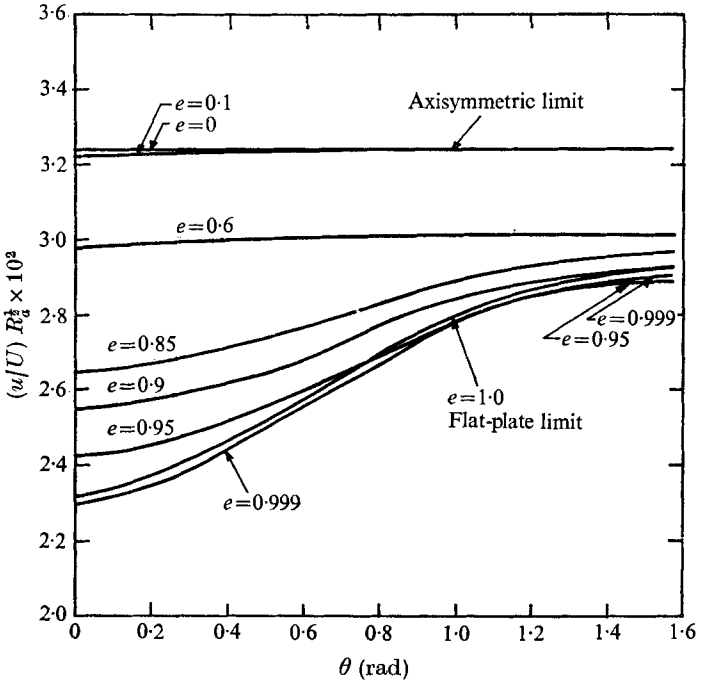

FIGURE 5. Streamwise perturbation. $a/s = 0{\cdot}1$.

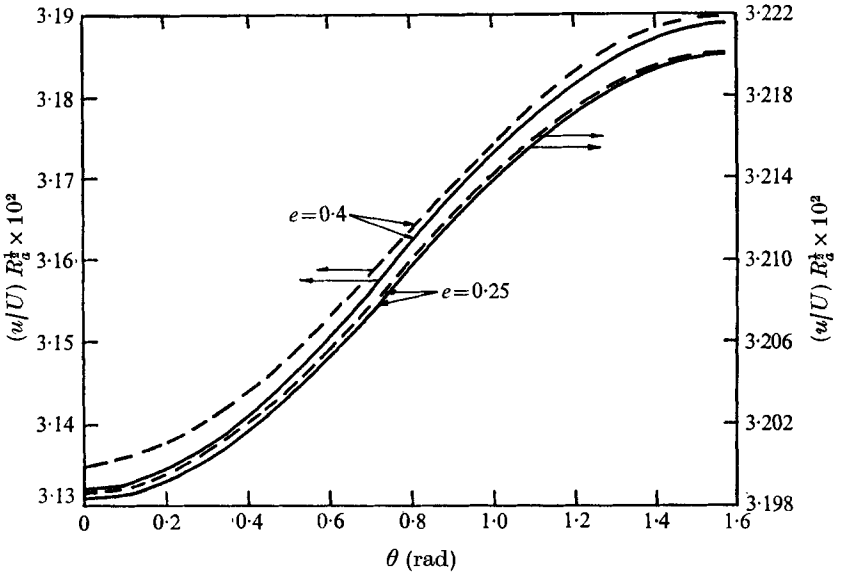

FIGURE 6. Streamwise perturbation. $a/s = 0{\cdot}1$. ——, numerical solution; – – –, quasi-axisymmetric theory, equation (18*a*). Right- and left-hand ordinate scales apply to right- and left-hand pairs of curves respectively.

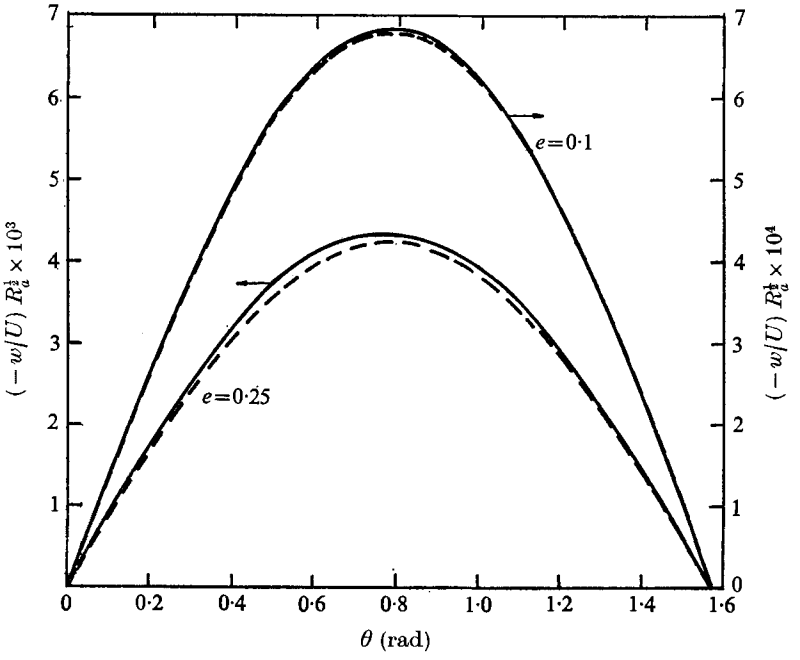

FIGURE 7. Cross-flow. $a/s = 0{\cdot}1$. ——, numerical solution; – – –, quasi-axisymmetric theory, equation (18*b*). Right- and left-hand ordinate scales apply to lower and upper pairs of curves respectively.

reduced to the consideration of a two-dimensional flow over an expanding body with porous boundary conditions. This results in a considerable simplification.

Complete solutions have been obtained for the flow over an elliptic cylinder in the form of a Fourier series. For the limiting cases of a finite-span flat plate and nearly circular geometry simplified analytic forms have been obtained. The surface solutions for the plate are in agreement with the exact three-dimensional result obtained by a simple extension of the method of Stewartson & Howarth (1960).

In the general case, a peak in the cross-flow velocity is predicted. The location of this maximum moves towards the side region of the ellipse as the eccentricity $e \to 1$. In this limit the cross-flow exhibits a logarithmic behaviour, corresponding to the flat-plate solutions, up to the peak location and then falls rapidly to zero at the symmetry line. For $e \to 1$, the application of a Blasius boundary condition near the edge is incorrect, as the transverse curvature is quite large there. Further studies will have to consider the side edge flow more exactly in order to determine the precise nature of the developing boundary region where curvature and cross-diffusion effects become important. It is believed that this slender-body procedure will be applicable to a wider class of cylindrical geometries where both the thin-boundary-layer and slender-body restrictions are satisfied.

This research was supported by the Air Force Office of Scientific Research, Office of Aerospace Research, under Grant AFOSR 70–1843, Project 9781–01.

The work reported here was based on part of a dissertation submitted by the second author to the faculty of the Polytechnic Institute of New York in partial fulfilment of the requirements for the Ph.D. degree (Aeronautics and Astronautics), 1974.

REFERENCES

ASHLEY, H. & LANDAHL, M. 1965 *Aerodynamics of Wings and Bodies.* Addison-Wesley.

COOKE, J. C. 1957 *Quart. J. Mech. Appl. Math.* **10**, 312–321.

GLAUERT, M. B. & LIGHTHILL, M. J. 1955 *Proc. Roy. Soc.* A **230**, 188–203.

GRADSHTEYN, I. S. & RYZHIK, I. M. 1965 *Tables of Integrals, Series, and Products.* Academic.

KAHANE, A. & SOLARSKI, A. 1953 *J. Aero. Sci.* **20**, 513–524.

PAL, A. & RUBIN, S. 1971 *Quart. Appl. Math.* **29**, 91–108.

RUBIN, S. 1966 *J. Fluid Mech.* **26**, 97–110.

RUBIN, S. & GROSSMAN, B. 1971 *Quart. Appl. Math.* **29**, 169–186.

RUBIN, S. & MUMMOLO, F. 1973 *Polytech. Inst. Brooklyn. PIBAL Rep.* no. 73–16.

SEBAN, R. A. & BOND, R. 1951 *J. Aero. Sci.* **18**, 671–675.

STEWARTSON, K. 1961 *J. Aero. Sci.* **28**, 1–10.

STEWARTSON, K. & HOWARTH, L. 1960 *J. Fluid Mech.* **7**, 1–21.

VAN DYKE, M. 1964 *Perturbation Methods in Fluid Mechanics.* Academic.

VAN DYKE, M. 1970 *6th U.S. Nat. Cong. Appl. Mech., Cambridge, Mass.*

WARD, G. N. 1955 *Linearized Theory of Steady, High Speed Flow.* Cambridge University Press.